ACS OMEGA

Open Access

http://pubs.acs.org/journal/acsodf

Article

Discerning Transuranic Sub-Concealments in Nuclear Waste Barrels Using γ-Ray Spectrometry: A Non-Invasive Assay Strategy To Combat the Threat of Nuclear Diversion

Sabyasachi Patra,* Satyam Kumar, and Rahul Tripathi

Cite This: *ACS Omega* 2024, 9, 44658−44667

Read Online

ACCESS | Metrics & More | Article Recommendations | Supporting Information

ABSTRACT: Insufficient inventory control arising from inadequate monitoring procedures can lead to vulnerabilities in nuclear security. In addition, insider threats, by either malicious intent or negligence, can pose a substantial risk by exploiting such deficiencies to perform unlawful actions, such as theft or diversion, which may lead to compromised nuclear security. Interim storage barrels, intended for temporary containment of low-density nuclear waste, require special attention in this regard. In certain scenarios, the inadequacy of the existing waste barrel assay methodologies to identify and correctly measure any undesirable transuranic subconcealment present inside may pose a risk of nuclear diversion. The present work aims to establish an absolute waste barrel assay procedure to mitigate such risks by offering a robust method for the detection and assay of transuranic subconcealments in nuclear waste barrels using high-resolution γ-ray spectrometry. Challenges related to the varying amounts of attenuation experienced by the γ-rays within the subconcealments, low-density matrix, and the steel barrel wall have been addressed by an iterative photopeak efficiency transfer approach. The methodology has been verified for the assay of seven mock-up samples mimicking nuclear diversion attempts using waste barrels, for which conventional barrel scanning would be inadequate and tomographic scanning would be highly time-consuming. Using this methodology, Pu and ^{241}Am isotopes have been assayed within <10% of the expected value for the majority, with the measurement uncertainty of <10%. The present method, which is simple and noninvasive, can identify inconsistencies with the labeled inventory and detect potential diversion attempts.

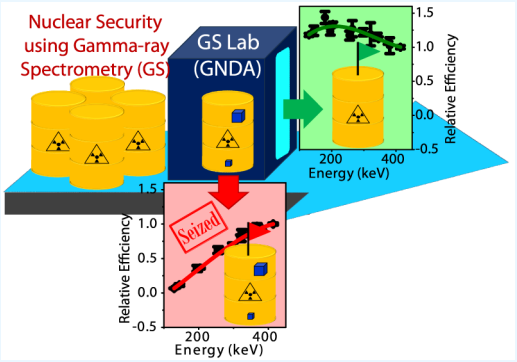

INTRODUCTION

Strengthening nuclear security and safeguarding infrastructure is given utmost priority in modern nuclear facilities. Frequent malicious incidents involving diversion of nuclear materials have been reported in the IAEA's incidents and trafficking database[1] in the recent past. Such incidences have prompted increasing research efforts toward developing methodologies for preventive detection to create deterrence for the diversion of special nuclear materials (SNMs) from nuclear facilities.[2−4] Advancement over the existing nuclear forensic methodologies is also needed for attribution of unknown nuclear materials out of regulatory control posing complex assay scenarios.[5−30] Interim storage of nuclear materials in a nuclear fuel cycle facility possesses the risk of diversion due to the presence of transuranic (TRU) elements containing fissile materials (for example, ^{239}Pu). Low and intermediate level solid wastes (LILW, 400−4000 Bq/g long-lived alpha emitters[31]) containing low to medium density scraps such as cellulose and fiber materials, protective rubber and plastic wear, used ion-exchange resins etc., in general, are contained in standard ∼200 L carbon steel barrels for interim storage. These special containers after filling with low-density solid nuclear scraps need to be inspected, classified, and assayed for TRU elements before sending them for further processing. Such large volume waste barrels are, in general, assayed by segmented gamma scanning (SGS), where the barrel is scanned for TRU nuclides segment by segment by a two pass relative assay procedure.[32,34]

The conventional SGS involves transmission measurements using an external γ-ray source for attenuation correction. We demonstrated in our previous work that, although the conventional SGS method with transmission-based attenuation correction works well for LILW barrels filled with low-density scraps containing radioactivity in dispersed form, it severely underestimates the assay results for samples containing actinide hot spots or lumps due to attenuation under-correction.[35,36] Hot spots may be visualized as localized actinide concentrations with considerably higher activity compared to the average bulk concentration (activity) in the

Received: August 12, 2024
Revised: October 7, 2024
Accepted: October 16, 2024
Published: October 24, 2024

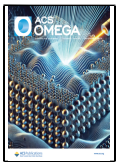

container. Considering a situation, for example, where a small packet containing few grams of PuO_2 powder is present inside a ∼200 L waste barrel, its self-attenuation (which is significant compared to the γ-ray attenuation in low Z and low-density bulk matrix) would be missed by the conventional transmission-based attenuation correction due to its insignificant volume (density of PuO_2 = 11.5 g/cm^3) compared to the waste barrel. This may result in an underestimation of the TRU amount/activity, which would increase the risk of diversion of TRU fissile isotopes (particularly ^{239}Pu) and any other radioisotopes, thereby posing a risk on nuclear security. This calls for a thorough inspection of the contents of the waste barrels using multiple techniques. In an alternative approach, if a simple, fast, and comprehensive noninvasive methodology is available to verify the labeled (declared) contents of a nuclear waste barrel to ensure nuclear safeguards and security, it would be highly beneficial.

Nondestructive radiometric methodologies, for example, high-resolution γ-ray spectrometry (HRGRS), often play a pivotal role in the elemental and isotopic assay in a variety of samples.[37−47] In particular, the passive HRGRS plays a significant role in nuclear waste assay due to its simplicity, reliability, nondestructive nature, and capability to assay the full sample volume in real time.[32−34,48−56] TRU elements (for example, Pu and Am) are normally present in different chemical forms (metal, oxide, and fluoride) and densities in research and production facilities involving nuclear fuel cycle activities. The γ-rays emitted from the isotopes of these elements experience significant self-attenuation due to their high Z when present in the waste barrel in lump/localized powder form or inside an illicit subconcealment (hot spots). In our previous work, we demonstrated that a suitable adaptation of the "apparent mass method" by Venkataraman and Croft[57] for segmented γ-ray assay eliminated the need for transmission-based attenuation correction and reasonably estimated plutonium lumps present in ∼200 L waste barrels.[36] However, such a methodology requires segmented scanning of the waste barrels using a slit collimated γ-ray spectrometer, which is a time-consuming assay procedure and not suitable for frequent routine safeguard verification exercises of waste barrels at the interim storage facility. Also, the "apparent mass method" requires a linear dependence of the apparent masses on the inverse of energy at minimum 4 to 5 spectral interference free γ-ray energies that limits its applicability to the samples with high γ-ray spectral interference and attenuation.[20]

The present work aims to provide a faster and simpler γ-ray-based methodology for safeguard verification of the LILW barrels at an interim storage facility with reasonable accuracy. A twin-detector assay setup with a rotating sample platform has been built for the γ-ray assay. The iterative γ-ray detection efficiency transfer methodology and the computer code (GNDA; Gamma-based Non-Destructive Assay code) developed earlier for in-field nuclear forensics of small volume sealed samples[19,20] have been extended for the assay of ∼200 L nuclear waste barrels by addressing additional problems related to nuclear waste barrel assay. Here, the γ-ray detection efficiency refers to the full energy peak (photopeak) efficiency. Unlike the previously reported nuclear forensic scenarios where the actinide self-attenuation and the container material attenuation governed the overall γ-ray attenuation and the absolute efficiency curve, the presence of a large quantity of low Z and low-density matrix in a ∼200 L nuclear waste barrel has a significant share in the overall γ-ray attenuation that has been taken into account during the efficiency transfer in the present work. The application of the proposed methodology has been demonstrated using several mock-up scenarios imitating the assay of nuclear waste barrels containing TRU hot spots or subconcealments, where multiple unknown sources of γ-ray attenuation have been corrected in an iterative way using the in-house code GNDA.

MATERIALS AND METHODS

Preparation of Mock-Up Samples and the Gamma-Ray Spectrometry Setup. Several small, sealed polypropylene containers with a known mass of plutonium oxide powder have been used to prepare mock-up nuclear waste barrels containing illicit TRU subconcealments as hot spots. The Pu oxide samples of known masses used in the present work have been made from previously reprocessed plutonium from the spent fuel of an Indian reactor. For radiological safety, the sealed polypropylene containers were further encapsulated in standard 250 mL plastic containers before insertion into the ∼200 L barrel. Five mock-up barrels with random and biased spatial distributions of the Pu subconcealments have been considered, with a total Pu of 10.75 g in the barrel. The Pu mass in an individual subcontainer has been kept below 1 g to prepare samples with a moderate self-attenuation effect within the actinide material, representing cases where the contribution of cellulose matrix attenuation to the overall γ-ray attenuation is substantial and needs to be corrected separately in addition to the actinide self-attenuation. In order to imitate more realistic diversion attempts, two additional mock-up barrels have been prepared with further complex assay scenarios, where all the small polypropylene subcontainers containing Pu have been placed inside a stainless steel canister, and the canister has been placed inside a ∼200 L barrel in varying spatial orientations. Shredded cellulose papers were used as the major matrix in the barrels. The total barrel mass, including cellulose, is about 40 kg, where the total cellulose mass in a barrel is about 15 kg.

In comparison to the traditional practice of relative SGS, where the sample and a standard barrel are scanned segment by segment using a slit-collimated high-purity germanium (HPGe) detector in a two pass (transmission and emission) approach, the present methodology is direct and based on absolute γ-ray spectrometry. As demonstrated in our previous studies, the spatial heterogeneity of the radioactivity distribution in a given sample can be addressed by a "varying distance approach", where the passive γ-rays emitted from the sample are measured at three different sample-to-detector distances. An estimate of the effective sample-to-detector distance for a given measurement geometry can thus be obtained in a numerical way.[19,20] In our earlier studies with small volume samples, it was convenient to move the samples for measurements at different distances while keeping the position of the detector fixed. Also, a single HPGe detector was used in our earlier studies, where the measurement at the largest sample-to-detector distance (25 cm) was used for the assay. Considering the difficulty in moving a ∼200 L waste barrel and also the HPGe detector with a 30 L liquid nitrogen dewar, it has been decided to introduce a dedicated mobile γ-ray spectrometer system in the present setup for the measurements at different distances in addition to the HPGe detector used for absolute assay. To this end, an $LaBr_3$ detector (SCINTIBLOC $LaBr_3$ detector, Saint − Gobain make) has been chosen considering its easy mobility and the reasonable

https://doi.org/10.1021/acsomega.4c07102
ACS Omega 2024, 9, 44658−44667

energy resolution (3.02% at 662 keV). A coaxial HPGe detector (50% relative efficiency with an energy resolution of 0.16% at 1332 keV, Baltic Scientific Instruments) has been used for acquiring a high-resolution γ-ray spectrum with reasonable statistics that has been used for the assay. Measurements using the $LaBr_3$ detector have been used to obtain the γ-ray count rate at 208 keV at three different sample-to-detector distances (measured sample-to-detector distances = 130, 90, and 60 cm), which were used to numerically obtain the effective sample-to-detector distance required for the absolute assay using the HPGe detector. The difference between the measured and the effective sample-to-detector distances (ΔR) for a heterogeneous sample can be obtained from eq S1 (see Section S3.1). In order to keep the effective sample-to-detector distance the same for the $LaBr_3$ and the HPGe detectors, the waste barrel has been rotated horizontally around its axis using a motorized platform during the measurement. Considering the large volume of the barrel (~200 L) and the large sample-to-detector distance (130 cm), it is reasonable to neglect the difference in the γ-ray mean free path in the HPGe and the $LaBr_3$ crystals of the respective detectors.

Figure 1 provides the 3D representation of the present experimental setup, where the HPGe and $LaBr_3$ detectors are

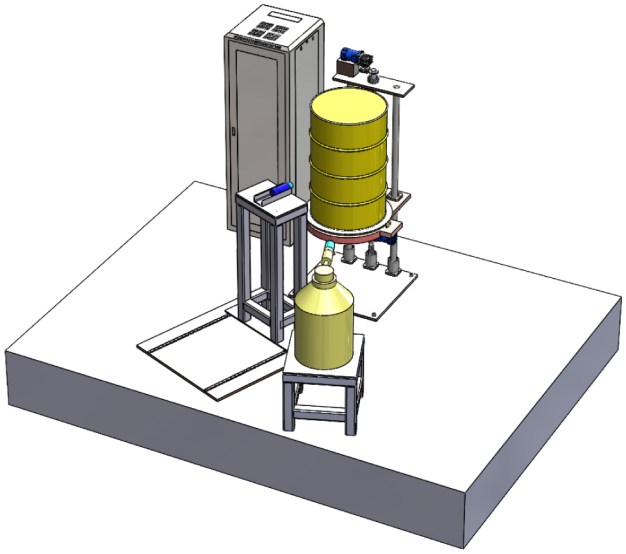

Figure 1. 3D representation of the present experimental setup.

angularly placed with respect to the barrel center at an approximate angle of 40°. The choice of the angle between the two detectors is arbitrary and can be varied depending on the convenience and available space in the laboratory. The barrel has been placed on a motorized rotary platform and rotated horizontally during the measurements at a rotation speed of 2.5 rpm. The barrel manipulator also includes a provision for vertical motion control. A detailed description of the experimental setup is provided in the Supporting Information, including the plan and elevation diagrams. The detector crystals have been covered with thin cadmium sheets (shown in cyan in Figure 1) to reduce the γ-ray counts at 59.5 keV of ^{241}Am.

Iterative Photopeak Efficiency Transfer: Extension of GNDA for Waste Barrel Assay. The present work is an extension of the iterative photopeak efficiency transfer methodology and the associated Python code (GNDA code) developed in our earlier studies for the assay of small volume sealed containments (250 mL to ~10 L).[19,20] In our previous investigations, the studies were focused on developing an "on-site" nondestructive methodology for in-field nuclear forensics of a suspected sealed package at borders or ports using HRGRS, where the samples were of nonstandard geometries and smaller in size. In such samples, the γ-ray attenuation mainly originated from actinide self-attenuation and unknown container material attenuation. Contrary to the nuclear forensic investigations of completely unknown samples, the assay of a nuclear waste barrel in the present work benefits from fairly available knowledge about its origin. Consequently, some assumptions about the attenuating materials can be made a priori for the waste barrel assay. For example, a typical LILW barrel in the nuclear industry contains low Z and low-density materials such as cellulose, polystyrene, neoprene, plastics, etc. as the major matrix and commonly called compressible waste. In common practice, compressible wastes are also categorized and segregated as cellulosic and noncellulosic classes. In general, the normal LILW barrels can be successfully assayed using the SGS methodology[32−34] relying on transmission-based attenuation correction procedures. However, as also demonstrated in our previous work for the SGS assay of waste barrel containing Pu lumps,[35,36] the transmission measurements would severely underestimate the effect of γ-ray attenuation within the localized TRU hot spots or subconcealments. In such SGS measurements, a strong variation of assay results with the γ-ray energy would work as a potential marker for the inadequate attenuation correction, suggesting further investigations. Such samples can be assayed using detailed tomographic scanning; however, it will be highly time-consuming and would require bulky instrumentation with 3D motion control.

In an alternative approach for faster assay, this problem can be addressed by extending the methodology proposed in our earlier studies.[19,20] In these studies with small volume samples,[19,20] the iterative photopeak efficiency transfer algorithm as implemented in GNDA showed strong potential to account for all different known and unknown sources of γ-ray attenuation. In order to adapt GNDA for a large volume waste barrel assay with possible complications such as the presence of subconcealments (hot spots), the methodology has been expanded further. In the present expansion, in addition to the actinide self-attenuation and the barrel wall attenuation, the attenuation due to the low Z and low-density matrix was also taken into account in an iterative way. Equation 1 gives the final derived expression for the GNDA-transformed absolute photopeak efficiency at a given γ-ray energy (E_i).

$$\varepsilon_{\mathrm{abs}}^{\mathrm{GNDA}}(E_i) = \varepsilon_{R_{\mathrm{eff}}}(E_i) \times e^{-\mu_L^{\mathrm{Cd}}(E_i)\times t_{\mathrm{Cd}}} \times e^{-\mu_L^{\mathrm{steel}}(E_i)\times t_{\mathrm{steel}}} \times \frac{\sum_{j=1}^{N} e^{-\mu_L^{\mathrm{TRU}}(E_i)\times x_j^{\mathrm{cum}}}}{N} \times e^{-\mu^{\mathrm{cell}}(E_i)/\rho_{\mathrm{cell}}\times(r+\Delta R)} \quad (1)$$

On the right side of eq 1, the first term ($\varepsilon_{R_{\mathrm{eff}}}(E_i)$) denotes the extended-source absolute photopeak efficiency without attenuation correction. The second term ($e^{-\mu_L^{\mathrm{Cd}}(E_i)\times t_{\mathrm{Cd}}}$) represents the correction due to γ-ray attenuation in the Cd filter of the known thickness (t_{Cd}). The third term ($e^{-\mu_L^{\mathrm{steel}}(E_i)\times t_{\mathrm{steel}}}$) represents the correction due to γ-ray

https://doi.org/10.1021/acsomega.4c07102
ACS Omega 2024, 9, 44658−44667

attenuation in the wall of steel barrel of known thickness (t_{steel}). The fourth term $\left(\frac{\sum_{j=1}^{N} e^{-\mu_L^{TRU}(E_i)\times x_j^{cum}}}{N}\right)$ represents the iterative TRU self-attenuation correction, where N parallel imaginary TRU slabs of thickness x_j have been considered with $Nx_j = X$, the effective TRU thickness. X is iteratively varied to match the simulated extended-source relative photopeak efficiency curve at no attenuation with the experimentally obtained relative photopeak efficiency data with the least chi-square. The γ-ray self-attenuation at different depths of the actinide ($\sum_1^j x_j$, termed as x_j^{cum}) has been jointly considered and included in the $\varepsilon_{abs}^{GNDA}(E_i)$. The last term in eq 1, $(e^{-\mu^{cell}(E_i)/\rho_{cell}\times(r+\Delta R)})$ represents the iterative correction term due to the low Z and low-density cellulose matrix, where, $\mu^{cell}(E_i)$ denotes the γ-ray energy dependent mass attenuation coefficient (cm^2/g) of cellulose, as obtained using the code MUPLOT.[58] The term "ρ_{cell}" stands for the cellulose density in g/cm^3, varied iteratively as a free parameter in the upgraded GNDA photopeak efficiency transfer. The term "r" denotes the inner radius of the steel barrel (28.1 cm in the present study) and "ΔR" denotes the numerically obtained positive or negative correction term mainly originating from the deviation between the C_G and C_R along the sample-to-detector axis (see Section S3.1 for details about ΔR, C_G, and C_R). The detailed stepwise discussion on the iterative methodology is given in the Supporting Information.

Safety Precautions. The present work has been carried out using sealed sources of plutonium oxide powder with the necessary protective clothing. All of the studies have been carried out in a dedicated radiological laboratory under radiation safety surveillance.

RESULTS AND DISCUSSION

In order to rule out insider threats during the interim storage of radioactive waste barrels, a rapid method for routine verification of the declared or labeled TRU amount is desirable. The results of the present investigation establish some experimental signatures to detect such diversion attempts and propose a simple and direct assay methodology for such samples, which is hitherto impossible by the conventional SGS methodology. Moreover, the simple and time-efficient GNDA methodology makes the routine verification of randomly picked waste barrels from the interim storage facility viable.

Experimental Signatures for the Presence of TRU Hot Spots in a Waste Barrel. Due to the wide variation in the energy-dependent attenuation coefficients for low and high Z materials, it is possible to identify the presence of high Z and high-density radioactive hot spots in the low Z and low-density matrix of an LILW barrel from the acquired γ-ray spectrometric data. The nature of the relative photopeak efficiency curve would clearly differentiate between the barrels containing uniformly distributed TRU activities and the barrels containing localized high-density hot spots. To understand this, γ-ray spectra in a 50% coaxial HPGe detector at a sample-to-detector distance of 130 cm were simulated using Geant4 Monte Carlo code for 214.5 L iron barrels having 10 g of Pu uniformly distributed in the cellulose matrix at two different bulk cellulose densities, such as 0.2 and 1.5 g/cm^3. The relative photopeak efficiency data for both cases, as obtained from simulation, have been coplotted along with the experimental relative photopeak efficiency data for a small volume Pu sample (a sealed sample containing 8.6 g of Pu as oxide powder) in Figure S4 . It may be noted that, when 10 g of Pu is uniformly distributed in a 214.5 L volume, the γ-ray self-attenuation within Pu is negligible due to the large dilution factor. Thus, in such samples, the γ-ray attenuation mainly originates from the low Z elements in the cellulose matrix. It is interesting to observe from Figure S4 that the localized distribution of Pu in a small volume exhibits a significantly higher energy-dependent variation in the relative photopeak efficiency profile compared to the cases when a similar mass of Pu is distributed uniformly in 214.5 L cellulose-filled barrels. For 8.6 g of the localized Pu sample, the photopeak efficiency at the lowest γ-ray energy (129.3 keV) used in the present study has been found to decrease by more than 90% with respect to the photopeak efficiency at 413.7 keV. On the contrary, for 10 g of distributed Pu samples in 214.5 L barrels, even at the cellulose density of 1.5 g/cm^3 (referring to a total cellulose mass of about 300 kg in the barrel), the photopeak efficiency at the lowest γ-ray energy (129.3 keV) decreases by only 20% with respect to the photopeak efficiency at 413.7 keV. For the cellulose density of 0.2 g/cm^3 (referring to a total cellulose mass of about 40 kg), the nature of the relative photopeak efficiency curve is different and shows a negligible effect of matrix attenuation. This suggests that the sensitivity of the dependence of the relative photopeak efficiency data on the γ-ray energy could be a potential experimental marker to recognize the absence or presence of high Z and high-density localized hot spots in a barrel under an assay. Additionally, the γ-ray energy-dependent bias on the assay result would also work as a marker of inadequate attenuation correction in the SGS assay, which will suggest the possible presence of TRU in the localized form or in the form of subconcealment.

Point Source Photopeak Efficiency Calibration. Considering the point-source photopeak efficiency at the geometric center of a given sample as a reasonable estimate of the respective extended-source photopeak efficiency at zero attenuation conditions (see Section S2 for validation of this approximation), the analysis in the present study starts with a Geant4 simulated photopeak efficiency curve for a point source at the geometric center of the ~200 L barrel without any attenuation. The details of Geant4 computations can be found in Section S2.

Description of the GNDA Code for Waste Barrel Assay. TRU elements in an LILW barrel may be present in a variety of forms, including chemical compounds or finely divided materials with varying densities. In the case of a diversion incidence, the container materials used for subconcealments could also vary in density and thickness. The potential of the GNDA methodology for handling such complex scenarios has been demonstrated in detail in our previous publications,[19,20] which can take care of the actinide self-attenuation and the unknown container material attenuation by an iterative photopeak efficiency transfer approach. For example, for a 10 mm thick Fe container (Z = 26), the GNDA methodology with iterative container attenuation correction could reproduce the assay result within 3% of the expected Pu mass with iteratively solved Fe thickness of 9.35 ± 0.45 mm.[19] In exceedingly complex situation, for example, Pu in a 10 mm thick Ta container (Z = 73), the assay result has been found to agree with the expected Pu mass within 13%, where the result without container attenuation correction would go enormously wrong (minimum by a factor of 4 in spite of using only the highest energy γ-ray).[19] This

https://doi.org/10.1021/acsomega.4c07102
ACS Omega 2024, 9, 44658−44667

demonstrates the prospective of the GNDA methodology and the code in handling exceptionally complicated attenuation scenarios, effectively. Importantly, the GNDA methodology does not need any previous assumption about the size, shape, physical, or chemical form of the sample including the density of the TRU material, which makes it flexible and largely adaptable. In the present work, in addition to the above-mentioned complexities as previously demonstrated with small volume samples,[19,20] the methodology and the code have been upgraded further for the absolute assay of TRU in a ∼200 L barrel. Additional challenges associated with complexities such as the presence of TRU hot spots (highly localized radioactivity distribution) and significant attenuation due to the large thickness of the low Z and low-density cellulose matrixes have been addressed. Scheme 1 gives a flowchart showing the sequence of steps in the upgraded GNDA analysis. A detailed description of each step can be found in detail in Section S3.

Assay of Mock-Up Barrels Containing TRU Hot Spots. As the present study has focused on developing a methodology for detecting potential nuclear diversion attempts using LILW barrels, mock-up samples have been prepared based on hypothetical arrangements of TRU subconcealments to represent different spatial distributions, extending from random to biased configurations. A large number of diversion scenarios may be anticipated using a nuclear waste barrel. For cases where the proportional contribution of low Z and low-density cellulose matrix on the overall γ-ray attenuation would be negligible, and the overall attenuation is mainly dominated by the sample self-attenuation and/or the unknown container material attenuation, the earlier version of the GNDA methodology would work.[19,20] However, when the sample self-attenuation and the container attenuation are not significantly high, the attenuation of γ-rays within the large thickness of low Z and low-density cellulose matrix also becomes significant and needs to be accounted separately in addition to the self-attenuation and container attenuation. The mock-up samples have been prepared to mimic such situations where the cellulose matrix attenuation is also significant in addition to the self-attenuation and container attenuation. As described in the Materials and Methods section, two different sets of mock-up samples have been prepared and subjected to the upgraded GNDA analysis (see Section S3 for the theoretical basis of the photopeak efficiency transfer in the upgraded GNDA code for waste barrel assay).

Scheme 1. Flow Chart Showing the Sequence of Steps Followed in the Upgraded GNDA Analysis for Waste Barrel Assay

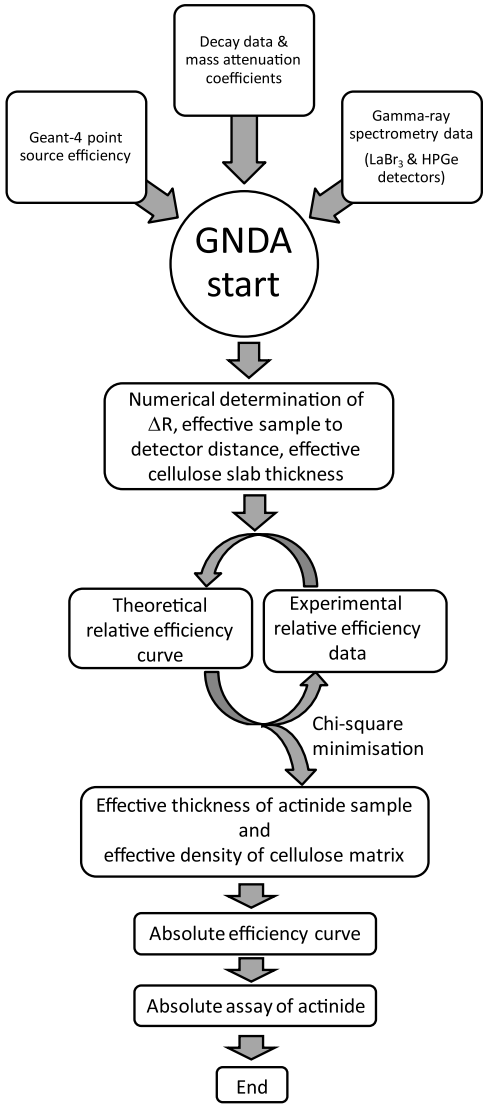

Set-I: Multiple TRU Hot Spots in Polypropylene Containers. In the first set, 20 small sealed polypropylene containers with a known mass of PuO_2 powder have been placed within the cellulose-filled barrel in five different spatial arrangements. Figure 2a−e illustrates various spatial distributions of the PuO_2 subconcealments in set-I mock-up barrels. Table S1 summarizes the numerically obtained ΔR values from the measurements using the $LaBr_3$ detector at varying sample-to-detector distances (see Section S3 for discussion on the determination of ΔR), where ΔR is a positive or negative distance parameter designating the difference between the geometric center (C_G) and the effective center of radioactivity (C_R) along the sample-to-detector axis in a rotating barrel (see Figure S3). The nonzero ΔR values suggest that the rotation of the barrel around the vertical axis in the present sample-to-detector geometry is not able to average out the radial inhomogeneity of the radioactivity distribution in the mock-up waste barrels. The negative ΔR values originate from the larger contribution of the measured γ-ray count rates from the proximal part of a rotating mock-up barrel compared to the rear part for the given sample-to-detector geometry. Hence, the value of $(R + \Delta R)$ gives the "effective" sample-to-detector distance for a rotating mock-up barrel under assay, where R denotes the measured sample-to-detector distance. Also, the value of $(r + \Delta R)$ gives the "effective" thickness of a cellulose slab (t_{cell}^{eff}) of unknown density placed between the C_R and the detector along the sample-to-detector axis, where r denotes the barrel radius (see the shaded thickness in Figure S3). The extended-source photopeak efficiency curves have thus been obtained using eq S2 and further converted into the respective absolute photopeak efficiency curves by the photopeak efficiency transfer procedure as implemented in the upgraded GNDA code while accounting for steel barrel wall attenuation, TRU self-attenuation and the cellulose matrix attenuation. The steel barrel attenuation correction has been straightforward due to the known wall thickness of the barrel. However, TRU

https://doi.org/10.1021/acsomega.4c07102
ACS Omega 2024, 9, 44658−44667

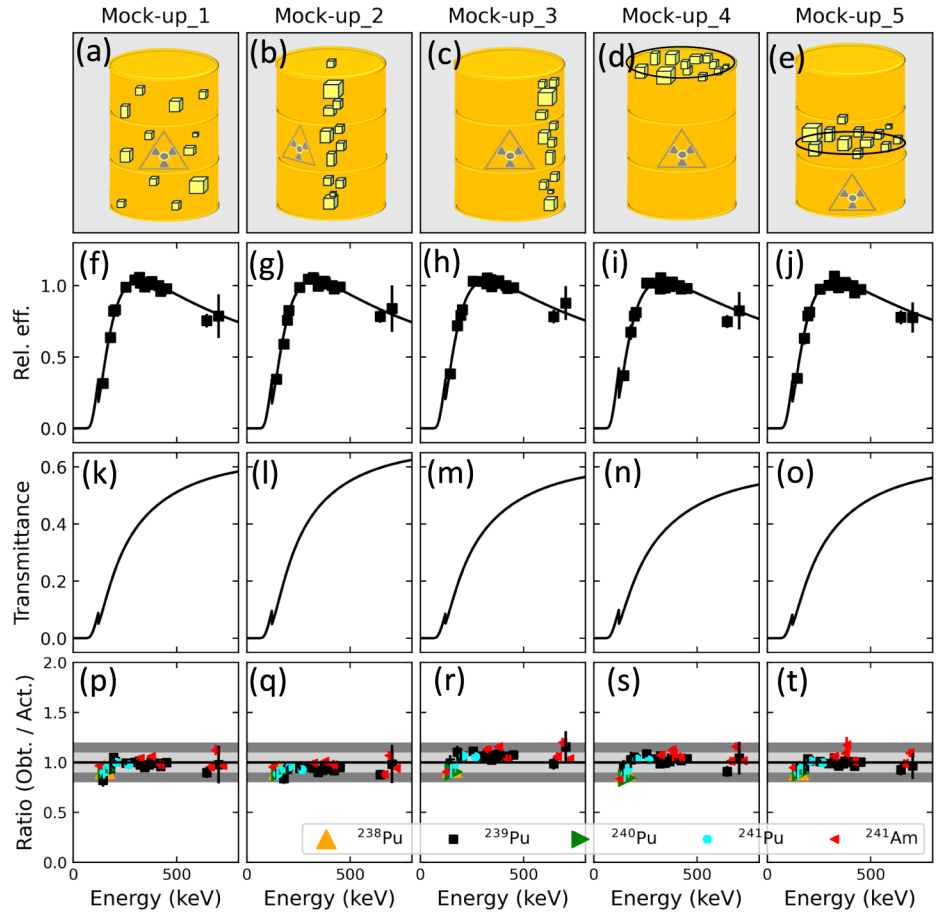

Figure 2. Schematic representation showing the spatial distribution of several Pu-containing polypropylene subconcealments (a−e) in 200 L barrels (the number and relative dimensions of the yellow boxes (subconcealments) inside the barrel are arbitrarily shown in the sketch), respective GNDA-transformed relative photopeak efficiency curve (solid line) and the relative efficiency data (f−j), respective transmission curve (k−o) and the ratio of obtained to the actual mass of Pu and ^{241}Am isotopes (p−t) for five different mock-up barrels in set-I of measurements. The error bars mostly originate from the propagation of uncertainties in the energy-dependent γ-ray count rates and the γ-ray abundances. For the majority of the data, the error bar is smaller than the size of the symbol and thus not visible. In p−t, the light and dark gray shades guide the eye for 10% and 20% uncertainty limits, respectively, for the expected ratio of obtained (Obt.) to the actual (Act.) mass (solid black line).

Table 1. Summary of the Effective Pu Thickness (cm), Effective Cellulose Slab Thickness (cm), and Effective Cellulose Density (g/cm^3) as Obtained from GNDA Analysis

	Set-I					Set-II	
	Mock-up_1	Mock-up_2	Mock-up_3	Mock-up_4	Mock-up_5	Mock-up_6	Mock-up_7
X_{Pu} (cm)	0.045	0.05	0.035	0.05	0.04	0.045	0.03
t_{cell}^{eff} (cm)	21.1	19.7	18.0	14.0	13.7	21.6	11.8
ρ_{cell} (g/cm^3)	0.21	0.21	0.31	0.46	0.41	0.26	0.66

self-attenuation and cellulose matrix attenuation have been solved iteratively.

Figure 2f−j shows the least chi-square fit of the experimentally obtained relative photopeak efficiency data with the respective GNDA-transformed relative photopeak efficiency curves. The iteratively obtained effective Pu thickness (X_{Pu}) and the effective cellulose density (ρ_{cell}) are given in Table 1. It can be seen that the X_{Pu} varies between 0.035 and 0.05 cm for all the samples in set-I of measurements. This variation can be attributed to the different effective path lengths traveled by the γ-rays within the Pu matrices at different sample-to-detector geometries (see Figure 2a−e for sample geometries). The effective thickness of the cellulose slab t_{cell}^{eff} (see Figure S3 for t_{cell}^{eff}) varies from 13.7 to 21.1 cm for different mock-up barrels of set-I under rotating sample-to-detector geometry. The iteratively obtained cellulose density (ρ_{cell}) has been found to vary between 0.21 and 0.46 g/cm^3, demonstrating the importance of the upgraded GNDA methodology for making a reasonable account of all of the different sources of the attenuation at a given sample-to-detector geometry. In this work, the large variation in the ρ_{cell} is attributed to the variation in the packing of the cellulose matrix, resulting in the variation in the γ-ray path length in the cellulose matrix and air for different sample-to-detector geometries. The γ-ray transmission curves for different mock-up barrels have been plotted in Figure 2k−o. Figure 2p−t gives

https://doi.org/10.1021/acsomega.4c07102
ACS Omega 2024, 9, 44658−44667

the ratio of the obtained masses to the actual masses of different TRU nuclides using different γ-ray energies. The results have been found to be reproduced within 10%. The γ-ray energy wise assay results are summarized in Tables S2−S6. The absence of energy-dependent bias corroborates a reasonable attenuation correction in such complex assay scenarios. A small systematic bias can be seen for mock-up_2 and 3, where the obtained results at all different γ-ray energies are positively or negatively biased within 10%. This deviation originates from the possible bias in the determination of ΔR by the varying distance approach for such large volume samples.

It may be noted that the effect of vertical inhomogeneity in obtaining ΔR was not significant in our earlier work[19,20] due to the smaller sample sizes. However, for a ∼200 L barrel, the vertical inhomogeneity wherever present may affect the ΔR measurement. This is due to the invalidity of the assumption of using the geometric center (C_G) of the barrel to obtain the effective sample-to-detector distances during ΔR determination (see Section S3.1 for the theory of ΔR measurements). Set-I measurements show that such an effect due to vertical inhomogeneity is not significant for samples containing dispersed hot spots. For mock-ups_2 and 3, the vertical inhomogeneity would have arisen from different amounts of Pu in different subcontainments placed vertically within the barrel leading to a systematic bias on the assay results (within 10%). This issue has been discussed more elaborately for set-II of mock-up samples, which have been prepared using a single hot spot. The effect of vertical inhomogeneity is more prominent for such samples, and a reasonable solution to this problem has been discussed therein.

Set-II: Concentrated and Localized TRU Hot Spots in a Stainless Steel Subconcealment. The potential of the upgraded GNDA code in reasonably assaying Pu in mock-up barrels containing multiple polypropylene subconcealments in various random and biased spatial distributions engenders an obvious curiosity to investigate it further for more complex scenarios, such as the presence of a single localized hot spot in a ∼200 L barrel filled with cellulose. The Pu sources in polypropylene packets, which were used to prepare the set-I mock-up barrels, have been placed together in a 1 mm thick stainless steel canister, providing additional complexity to the assay. For these highly localized hot spots, the ΔR calculation using eq S1 may introduce a larger systematic bias in the GNDA results. To circumvent this problem, the mock-up barrels have been quickly screened axially using the $LaBr_3$ detector prior to assay, and the height corresponding to the maximum γ-ray count rate is obtained (see the coordinate $C_{G'}$ in Figure S5). Figure S5 displays an example in which the hot spot is located far from the geometric center, axially. The measured sample-to-detector distances (R) in eq S1 can be modified as $\sqrt{R^2 + \Delta H^2}$, where ΔH denotes the axial difference between the $C_{G'}$ and C_G (see Figure S5). Thus, eq S1 modifies to

$$\frac{CR_{208}^{R_1}}{CR_{208}^{R_2}} = \left(\frac{\sqrt{R2^2 + \Delta H^2} + \Delta R}{\sqrt{R1^2 + \Delta H^2} + \Delta R} \right)^2 \quad (2)$$

Figure 3a,b schematically shows the spatial distribution of the Pu-containing stainless steel subconcealments in the set-II mock-up barrels. The quick axial scans shown in Figure 3c,d clearly suggest the localized radioactivity distribution in the

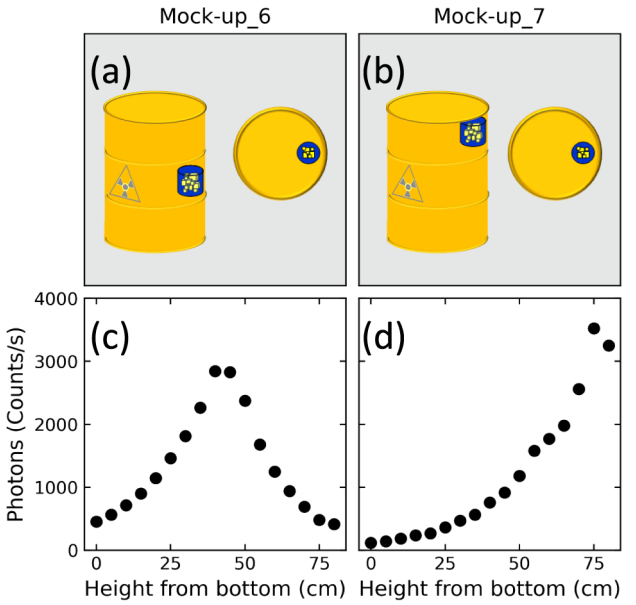

Figure 3. Schematic representation showing the spatial organization of the single Pu subconcealment in stainless steel (a,b), and the respective axial fast scanning profile using the $LaBr_3$ detector (c,d). The livetime of measurements at each height was 10 s. The detected photon counts per second at 208 keV at different heights from the bottom have been plotted. The error bar due to counting statistics is smaller than the size of the symbol and thus not visible in c,d. The stainless steel subconcealment is shown in blue color containing PuO_2 pouches (yellow boxes) inside (a,b). The relative dimension of the subconcealment inside the barrel is arbitrarily displayed in the sketch.

samples. While Figure 3c suggests the center of radioactivity (C_R) to be present somewhere in the mid-height of the barrel, Figure 3d clearly points to the C_R being present somewhere close to the top surface of the barrel, which suggests the need for eq 2 for the determination of ΔR. The numerically obtained ΔR values are summarized in Table S1. Figure 4a,b give the GNDA transformed relative photopeak efficiency curve and the experimentally obtained relative photopeak efficiency data for mock-ups_6 and 7. The iteratively obtained effective Pu thickness (X_{Pu}) and the effective cellulose density (ρ_{cell}) for set-II of the measurements are also summarized in Table 1. The transmission curves for the same have been plotted in Figure 4c,d. Figure 4e,f gives the ratio of obtained (Obt.) to actual (Act.) mass of different isotopes in the set-II of mock-up samples as obtained by the upgraded GNDA analysis. The energy-wise assay results are summarized in detail in Tables S7 and S8. Table 2 summarizes the error weighted mean masses (g) of different isotopes in the mock-up samples as obtained using the upgraded GNDA analysis.

Usefulness and Limitations in Comparison to the State-of-the-Art Techniques. The upgraded GNDA methodology, as demonstrated in this work, is a direct and absolute assay methodology for nuclear waste barrels. Unlike the apparent mass method, which requires a good number of interference-free γ-ray energies to be detected, GNDA can work, in principle, with γ-rays at only two energies (of course, the larger the number of γ-ray energies, the better the quality of iterative relative photopeak efficiency fitting in GNDA). Moreover, the GNDA methodology and the code can be used for heavily attenuating samples, where an infinite thickness condition is attained for the lower energy γ-rays. The code

https://doi.org/10.1021/acsomega.4c07102
ACS Omega 2024, 9, 44658−44667

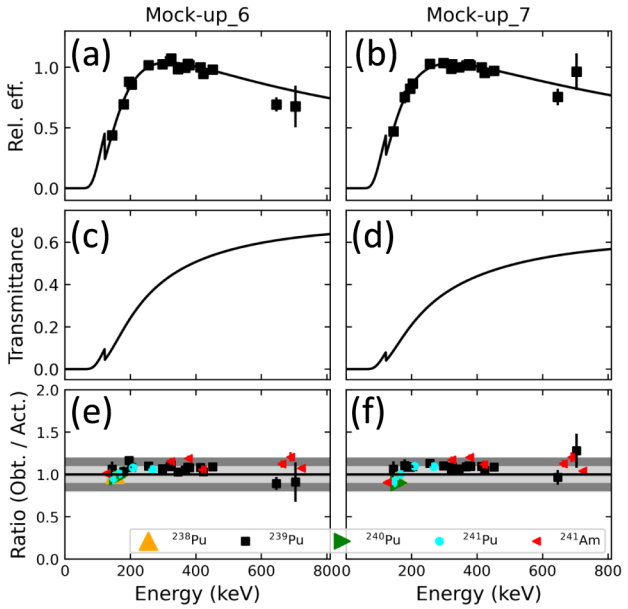

Figure 4. GNDA-transformed relative photopeak efficiency curve (solid line) and the relative photopeak efficiency data (a,b), respective transmission curve (c,d), and the ratio of obtained (Obt.) to the actual (Act.) mass of Pu and ^{241}Am isotopes (e,f) for two different mock-up barrels in set-II of measurements. The error bars majorly originate from the propagation of uncertainties in the energy-dependent γ-ray count rates and the γ-ray abundances. For the majority of the data, the error bar is smaller than the size of the symbol and thus not visible.

addresses the effect of sample heterogeneity as well as different sources of attenuation, such as TRU self-attenuation, cellulose matrix attenuation, and container wall attenuation, in an iterative way. Being coded in Python, the entire data analysis takes less than 5 min and is thus suitable for routine safeguard verification exercises at the interim storage facility. Certainly, like all other γ-ray spectrometry-based methodologies, the current methodology would fail for barrels containing infinitely thick TRU blocks as hot spots or TRU inside extremely heavy shielding. However, such a situation can be recognized much more easily from the difference in neutron and gamma responses, and appropriate procedures such as neutron assay of individual packets in the barrel can be carried out.

CONCLUSIONS

The conventional SGS methodology may severely underestimate the TRU isotopes when present as hot spots due to the underestimation of the attenuation, thereby posing a nuclear security challenge. In this work, an absolute and direct γ-ray assay methodology has been proposed for inventory controls and monitoring of large volume LILW barrels kept at an interim storage facility with the objective of combating nuclear diversion attempts using waste barrels. It has been demonstrated that high-resolution γ-ray spectrometry may offer obvious qualitative signatures for the presence of high-density radioactive hot spots in a waste barrel. The challenges associated with the γ-ray attenuation correction and absolute photopeak efficiency calibration have been addressed, and a reasonably accurate assay of TRU isotopes has been achieved. The methodology is based on an iterative photopeak efficiency transfer approach, where the γ-ray attenuation within the high

Table 2. Error Weighted Mean Masses (g) of the Mock-Up Samples as Obtained Using the Upgraded GNDA Analysis

	Sample	Isotope	[a]Obtained (Obt.) mass (g)	% Deviation $\left(\frac{\text{Obt.}-\text{Act.}}{\text{Act.}} \times 100\right)$
set-I	mock-up_1	^{238}Pu	0.0140 ± 0.0005	−6.7
		^{239}Pu	7.44 ± 0.38	−1.2
		^{240}Pu	2.59 ± 0.08	−7.6
		^{241}Pu	0.187 ± 0.007	−2.6
		[b]total Pu	10.23 ± 0.39	−4.8
		^{241}Am	0.111 ± 0.006	1.0
	mock-up_2	^{238}Pu	0.0139 ± 0.0004	−7.3
		^{239}Pu	7.03 ± 0.26	−6.6
		^{240}Pu	2.53 ± 0.07	−9.7
		^{241}Pu	0.180 ± 0.005	−6.3
		[b]total Pu	9.75 ± 0.27	−9.3
		^{241}Am	0.107 ± 0.006	−2.7
	mock-up_3	^{238}Pu	0.0142 ± 0.0005	−5.3
		^{239}Pu	8.00 ± 0.29	6.2
		^{240}Pu	2.54 ± 0.09	−9.4
		^{241}Pu	0.199 ± 0.012	3.6
		[b]total Pu	10.75 ± 0.30	0.0
		^{241}Am	0.117 ± 0.010	6.4
	mock-up_4	^{238}Pu	0.0137 ± 0.0005	−8.7
		^{239}Pu	7.76 ± 0.32	3.1
		^{240}Pu	2.37 ± 0.08	−15.4
		^{241}Pu	0.193 ± 0.013	0.5
		[b]total Pu	10.34 ± 0.33	−3.8
		^{241}Am	0.113 ± 0.010	2.7
	mock-up_5	^{238}Pu	0.0138 ± 0.0005	−8.0
		^{239}Pu	7.52 ± 0.25	−0.1
		^{240}Pu	2.52 ± 0.08	−10.1
		^{241}Pu	0.190 ± 0.009	−1.0
		[b]total Pu	10.24 ± 0.26	−4.7
		^{241}Am	0.114 ± 0.008	3.6
set-II	mock-up_6	^{238}Pu	0.0150 ± 0.0005	0.0
		^{239}Pu	8.10 ± 0.49	7.6
		^{240}Pu	2.73 ± 0.07	−2.6
		^{241}Pu	0.202 ± 0.009	5.2
		[b]total Pu	11.05± 0.50	2.7
		^{241}Am	0.122 ± 0.007	10.9
	mock-up_7	^{238}Pu	0.0148 ± 0.0006	−1.3
		^{239}Pu	8.21 ± 0.44	9.0
		^{240}Pu	2.52± 0.09	−10.1
		^{241}Pu	0.205 ± 0.014	6.8
		[b]total Pu	10.95± 0.45	1.8
		^{241}Am	0.119 ± 0.011	8.2

[a]Error weighted mean mass ± measurement uncertainty for multiple γ-ray emitting isotopes (see the Supporting Information for assay results at different γ-ray energies). [b]Total Pu excludes ^{242}Pu (typical abundance of <3% in power reactor grade Pu), which could not be assayed by HRGRS due to the absence of detectable γ-rays. The known actual (Act.) masses of different isotopes in a given mock-up barrel are ^{238}Pu = 0.015 g, ^{239}Pu = 7.530 g, ^{240}Pu = 2.803 g, ^{241}Pu = 0.192 g, ^{242}Pu = 0.213 g, and ^{241}Am = 0.110 g.

https://doi.org/10.1021/acsomega.4c07102
ACS Omega 2024, 9, 44658−44667

Z and high-density actinide particles (described as self-attenuation) and within the low Z and low-density cellulose matrix has been determined by an iterative procedure and used for the transfer of point to extended-source absolute efficiencies without requiring any prior information about the presence or absence of TRU hot spots in a barrel. It is also independent of size, shape, spatial distribution, and the physicochemical form of the TRU hot spots that may be present in a waste barrel. In the present work, with various mock-up barrels mimicking diversion scenarios, it has been demonstrated that the present assay methodology gives an estimate of the total Pu within 10% with a maximum measurement uncertainty of 10%, suggesting its potential use for periodic inventory verification of labeled waste barrels in an interim storage facility. The limit of detection for ^{239}Pu has been determined for the present assay setup and has been found to be 36 mg. The methodology has been made easily transferable by means of an in-house Python code that can be easily trained to an operator. Of course, it can also be a potential substitute for the well-accepted practice of SGS for routine waste barrel assays when faster assay is required. In conclusion, the development of a methodology for the detection and assay of TRU hot spots (subconcealments) in nuclear waste barrels represents an important attempt toward combating nuclear diversion, enhancing nuclear security, and pushing the boundaries of nuclear forensic and safeguard capabilities.

■ ASSOCIATED CONTENT

Supporting Information

The Supporting Information is available free of charge at https://pubs.acs.org/doi/10.1021/acsomega.4c07102.

Description of the present system; Geant4 computation; theoretical basis of efficiency transfer for the assay of hot spots in a ∼200 L barrel; experimental signatures for the presence of hot spots in a waste barrel; numerically obtained ΔR values; γ-ray energy-dependent assay results; axial scanning of barrels using an $LaBr_3$ detector and the modified C_G; quantitative ability and assay time requirement (PDF)

■ AUTHOR INFORMATION

Corresponding Author

Sabyasachi Patra − *Radiochemistry Division, Bhabha Atomic Research Centre, Mumbai 400085, India; Homi Bhabha National Institute, Mumbai 400094, India;* orcid.org/0000-0003-1880-195X; Email: spatra@barc.gov.in, sspatra86@gmail.com

Authors

Satyam Kumar − *Radiochemistry Division, Bhabha Atomic Research Centre, Mumbai 400085, India*

Rahul Tripathi − *Radiochemistry Division, Bhabha Atomic Research Centre, Mumbai 400085, India; Homi Bhabha National Institute, Mumbai 400094, India*

Complete contact information is available at: https://pubs.acs.org/10.1021/acsomega.4c07102

Author Contributions

The manuscript has been prepared using contributions from all authors.

Notes

The authors declare no competing financial interest.

■ ACKNOWLEDGMENTS

The authors thank Dr. P.K. Mohapatra, former Director, Radiochemistry & Isotope Group, and former Head, Radiochemistry Division, BARC, for his keen interest in this work. Sincere thanks to Dr. Saurabh Mukherjee for creating the 3D representation and the plan and elevation diagrams of the experimental setup.

■ REFERENCES

(1) IAEA. *Incident and Trafficking Database (ITDB)*. https://www.iaea.org/resources/databases/itdb.

(2) IAEA. *Safeguards techniques and equipment*; IAEA: Vienna, Austria, 2003, Vol. *1*

(3) IAEA. *Detection of radioactive materials at borders*; IAEA: Vienna, Austria, 2002.

(4) Zebroski, E. L. Analysis of risks of diversion of plutonium or highly enriched uranium In *Uncertainty in risk assessment, risk management, and decision making. Advances in risk analysis* Covello, V. T.; Lave, L. B.; Moghissi, A.; Uppuluri, V. R. R., Eds.; Springer: Boston, MA, 1987, Vol. *4*.

(5) Mayer, K. Security: Expand nuclear forensics. *Nature* **2013**, *503*, 461−462.

(6) May, M.; Davis, J.; Jeanloz, R. Preparing for the worst. *Nature* **2006**, *443*, 907−908.

(7) Kristo, M. J.; Gaffney, A. M.; Marks, N.; Knight, K.; Cassata, W. S.; Hutcheon, I. D. Nuclear forensic science: Analysis of nuclear material out of regulatory control. *Annu. Rev. Earth Planet. Sci.* **2016**, *44*, 555−579.

(8) Straub, M. D.; Arnold, J.; Fessenden, J.; Kiplinger, J. L. Recent advances in nuclear forensic chemistry. *Anal. Chem.* **2021**, *93*, 3−22.

(9) Hansona, S. K.; Pollington, A. D.; Waidmann, C. R.; Kinman, W. S.; Wende, A. M.; Miller, J. L.; Berger, J. A.; Oldhama, W. J.; Selby, H. D. Measurements of extinct fission products in nuclear bomb debris: Determination of the yield of the Trinity nuclear test 70 y later. *Proc. Natl. Acad. Sci. U.S.A.* **2016**, *113* (29), 8104−8108.

(10) Fahey, A. J.; Zeissler, C. J.; Newbury, D. E.; Davis, J.; Lindstrom, R. M. Postdetonation nuclear debris for attribution. *Proc. Natl. Acad. Sci. U.S.A.* **2010**, *107* (47), 20207−20212.

(11) Mayer, K.; Wallenius, M.; Varga, Z. Interviewing a silent (radioactive) witness through nuclear forensic analysis. *Anal. Chem.* **2015**, *87*, 11605−11610.

(12) Varga, Z.; Wallenius, M.; Krachler, M.; Rauff-Nisthar, N.; Fongaro, L.; Knott, A.; Nicholl, A.; Mayer, K. Trends and perspectives in nuclear forensic science. *Trends Anal. Chem.* **2022**, *146*, 116503.

(13) Mayer, K.; Wallenius, M.; Varga, Z. Nuclear forensic science: Correlating measurable material parameters to the history of nuclear material. *Chem. Rev.* **2013**, *113*, 884−900.

(14) Keegan, E.; Kristo, M. J.; Toole, K.; Kips, R.; Young, E. Nuclear forensics: Scientific analysis supporting law enforcement and nuclear security investigations. *Anal. Chem.* **2016**, *88*, 1496−1505.

(15) Reilly, S. D.; Patton, G. M.; Murillo, J.; Oldham, W. J.; Miller, J. L.; LaMont, S. P.; Sanborn, M. E.; May, I.; Gaunt, A. J.; Hanson, S. K. Trace actinide signatures of a bulk neptunium sample. *Anal. Chem.* **2023**, *95*, 9123−9129.

(16) Mayer, K.; Wallenius, M.; Ray, I. Nuclear forensics - a methodology providing clues on the origin of illicitly trafficked nuclear materials. *Analyst* **2005**, *130*, 433−441.

(17) Mayer, K.; Wallenius, M.; Lutzenkirchen, K.; Horta, J.; Nicholl, A.; Rasmussen, G.; Belle, P.; Varga, Z.; Buda, R.; Erdmann, N.; et al. Uranium from German nuclear power projects of the 1940s - a nuclear forensic investigation. *Angew. Chem. Int. Ed.* **2015**, *54*, 13452−6.

(18) Norman, E. B.; Thomas, K. J.; Telhami, K. E. Seaborg's plutonium? a case study in nuclear forensics. *Am. J. Phys.* **2015**, *83*, 843−845.

(19) Patra, S.; Mani, A. M.; Kumar, S.; Tripathi, R. Interrogating a mixed actinide basket using high-resolution γ-ray spectrometry: A nuclear forensic perspective on possible smuggling scenarios. *Anal. Chem.* **2024**, *96* (7), 2857−2865.
(20) Kumar, S.; Patra, S.; Mhatre, A.; Tripathi, R. In view of "on-site" nuclear forensics and assay of fissile materials in sealed packages by high-resolution γ-ray spectrometry. *Anal. Chem.* **2023**, *95* (6), 3247−3254.
(21) Patra, S.; Tripathi, R.; Pujari, P. K. Application of gamma-ray spectrometry, neutron multiplicity counting and calorimetry for non-destructive assay of U-Pu mixed samples. *Appl. Radiat. Isot.* **2021**, *176*, 109891.
(22) O'Neal, P. J.; Chirayath, S. S. Separated plutonium attribution using machine learning techniques. *Trans. Am. Nucl. Soc.* **2021**, *124*, 428−431.
(23) O'Neal, P. J.; Chirayath, S. S.; Cheng, Q. A machine learning method for the forensics attribution of separated plutonium. *Nucl. Sci. Eng.* **2022**, *196*, 811−823.
(24) Kitcher, E. D.; Osborn, J. M.; Chirayath, S. S. Characterization of plutonium for nuclear forensics using machine learning techniques. *Ann. Nucl. Energy* **2022**, *170*, 108987.
(25) Glennon, K. J.; Bond, E. M.; Bredeweg, T. A.; Chirayath, S. S.; O'Neal, P. J.; Folden, C. M. Nuclear forensics methodology identifies legacy plutonium from the Manhattan Project. *J. Radioanal. Nucl. Chem.* **2021**, *330*, 57−65.
(26) Martinson, S. P.; Garcia, J. R.; Haynes, I. W.; Saini, S. P.; Wagner, E. R.; Long, G. R.; Folden Iii, C. M.; Chirayath, S. S. Nondestructive and destructive assay for forensics characterization of weapons-grade plutonium produced in LEU irradiated in a thermal neutron spectrum. *Ann. Nucl. Energy* **2023**, *183*, 109645.
(27) Lloyd, C.; Goddard, B. Impacts of gamma ray emissions of materials containing ^{232}U on safety, security, and safeguards. *Nucl. Eng. Des.* **2020**, *370*, 110905.
(28) Lloyd, C.; Goddard, B. Ability of non-destructive assay techniques to identify sophisticated material partial defects. *Nucl. Eng. Technol.* **2020**, *52*, 1252−1258.
(29) Lützenkirchen, K.; Wallenius, M.; Varga, Z.; Wiss, T.; Knott, A.; Nicholl, A.; Mayer, K. Nuclear forensics on uranium fuel pellets. *Radiochim. Acta* **2019**, *107* (7), 635−643.
(30) Wallenius, M.; et al. Nuclear forensic investigations with a focus on plutonium. *J. Alloys Compd.* **2007**, *444*−*445*, 57−62.
(31) Wattal, P. K. Indian programme on radioactive waste management, Sadhana - Indian Academy of Sciences. *Sadhana* **2013**, *38* (5), 849−857.
(32) Eccleston, G. W. *Segmented gamma-ray scanner*; Los Alamos National Laboratory, 1991.
(33) Martin, E. R.; Jones, D. F.; Parker, J. L. *Gamma-ray measurements with the segmented gamma scan*; Los Alamos National Laboratory, 1977.
(34) Patra, S.; Agarwal, C.; Mhatre, A.; Goswami, A.Development of segmented gamma-ray scanning (SGS) system for the assay of low level nuclear waste (LLW) in 200 L drums. In *Proceedings of the twelfth DAE-BRNS national symposium on nuclear and radiochemistry*, INIS Reference Number 46089801, IAEA, 2015.
(35) Patra, S.; Agarwal, C.; Chaudhury, S. Full energy peak efficiency calibration for the assay of large volume radioactive waste drums in a segmented gamma scanner. *Appl. Radiat. Isot.* **2019**, *144*, 80−86.
(36) Patra, S.; Agarwal, C. Segmented gamma-ray assay of large volume radioactive waste drums containing plutonium lumps. *Appl. Radiat. Isot.* **2019**, *153*, 108827.
(37) Salutsky, M. L.; Curtis, M. L.; Shaver, K.; Elmlinger, A.; Miller, R. A. Determination of protactinium by gamma spectrometry. *Anal. Chem.* **1957**, *29* (3), 373−375.
(38) Phillips, J. R.; Waterbury, G. R.; Vanderborgh, N. E.; Marshall, T. K. Quantitative determination of fission products in irradiated fuel pins using nondestructive gamma scanning. *Anal. Chem.* **1975**, *47* (1), 71−75.
(39) Revay, Z. Determining elemental composition using prompt γ activation analysis. *Anal. Chem.* **2009**, *81*, 6851−6859.
(40) Huszank, R.; Csedreki, L.; Torok, Z. Direct trace element analysis of liquid blood samples by in-air ion beam analytical techniques (PIXE−PIGE). *Anal. Chem.* **2017**, *89*, 1558−1564.
(41) Kucera, J.; Bennett, J. W.; Oflaz, R.; Paul, R. L.; De Nadai Fernandes, E. A.; Kubesova, M.; Bacchi, M. A.; Stopic, A. J.; Sturgeon, R. E.; Grinberg, P. Elemental characterization of single-wall carbon nanotube certified reference material by neutron and prompt γ activation analysis. *Anal. Chem.* **2015**, *87*, 3699−3705.
(42) Toh, Y.; Segawa, M.; Maeda, M.; Tsuneyama, M.; Kimura, A.; Nakamura, S.; Endo, S.; Ebihara, M. Nondestructive quantitative analysis of difficult-to-measure radionuclides ^{107}Pd and ^{99}Tc. *Anal. Chem.* **2021**, *93*, 9771−9777.
(43) D'Agostino, G.; Luzio, M. D.; Mana, G.; Oddone, M.; Pramann, A.; Prata, M. ^{30}Si mole fraction of a silicon material highly enriched in ^{28}Si determined by instrumental neutron activation analysis. *Anal. Chem.* **2015**, *87*, 5716−5722.
(44) Kaste, J. M.; Bosticka, B. C.; Heimsath, A. M. Determining ^{234}Th and ^{238}U in rocks, soils, and sediments via the doublet gamma at 92.5 keV. *Analyst* **2006**, *131* (6), 757−763.
(45) El-Daoushy, F.; Hernández, F. Gamma spectrometry of ^{234}Th (^{238}U) in environmental samples. *Analyst* **2002**, *127*, 981−989.
(46) Parus, J. L.; Raab, W.; Doubek, N.; Zahradnik, P.; Deron, S. Comparison of two radiometric methods for the determination of americium-241 in plutonium containing materials. *Analyst* **1989**, *114*, 275−277.
(47) Lakosi, L.; Zsigrai, J.; Kocsonya, A.; Nguyen, T. C.; Rameback, H.; Parsons-Moss, T.; Gharibyan, N.; Moody, K. Gamma spectrometry in the ITWG CMX-4 exercise. *J. Radioanal. Nucl. Chem.* **2018**, *315*, 409−416.
(48) Bjork, C. W. Current segmented gamma scanner technology. In *Proceedings of 3rd International Conference on Facility Operation Safeguards Interface*, IAEA, 1987.
(49) Sprinkle Jr, J. K.; T-Hsue, S. *Recent advances in segmented gamma scanner analysis*, Los Alamos National Laboratory, LA-UR-87−3954, 1987.
(50) Mason, J. A., et al. A Tomographic segmented gamma scanner for the measurement of decommissioning wastes. In *Proceedings of ICEM03*; Examination School: Oxford, England, 2003
(51) Bai, Y. F.; Mauerhofer, E.; Wang, D. Z.; Odoj, R. An improved method for the non-destructive characterization of radioactive waste by gamma scanning. *Appl. Radiat. Isot.* **2009**, *67*, 1897−1903.
(52) Flis, P. Relation between the activity of a high-density waste drum and its gamma count rate measured with an unshielded Ge-detector. *Appl. Radiat. Isot.* **1995**, *46* (8), 805−812.
(53) Thanh, T. T.; Trang, H. T. K.; Chuong, H. D.; Nguyen, V. H.; Tran, L. B.; Tam, H. D.; Tao, C. V. A prototype of radioactive waste drum monitor by non-destructive assays using gamma spectrometry. *Appl. Radiat. Isot.* **2016**, *109*, 544−546.
(54) Cesana, A.; Terrani, M.; Sandrelli, G. Gamma activity determination in waste drums from nuclear plants. *Appl. Radiat. Isot.* **1993**, *44*, 517−520.
(55) Krings, T.; Mauerhofer, E. Reconstruction of the activity of point sources for the accurate characterization of nuclear waste drums by segmented gamma scanning. *Appl. Radiat. Isot.* **2011**, *69*, 880−889.
(56) Curtis, D. *Advancements in nuclear waste assay*, Ph.D thesis; University of Birmingham, 2007.
(57) Venkataraman, R.; Croft, S. Determination of plutonium mass using gamma-ray spectrometry. *Nucl. Instr. Meth. Phys. Res., A* **2003**, *505*, 527−530.
(58) *MUPLOT: A software tool for the computation of x-ray attenuation coefficients*, Università di Bologna, 2006. http://shape.ing.unibo.it/html/muplot.htm.

https://doi.org/10.1021/acsomega.4c07102
ACS Omega 2024, 9, 44658−44667